ISSN (Print) 1226-1750
ISSN (Online) 2233-6656
Journal of Magnetics 31(3), 333-339 (2026) https://doi.org/10.4283/JMAG.2026.31.3.333

Effect of Boron Substitution on Magnetic Properties and Magnetic Domain Behavior of $Fe_{62-x}Co_{25}Ti_7Zr_6B_x$ Amorphous Alloys

Hayan Shin[1], Hyunkyung Lee[1], Priyanka Das[2], Dong-Hyun Kim[2], and Haein Choi-Yim[1,3]*

[1]*Department of Applied Physics, Sookmyung Women's University, Seoul 04310, Republic of Korea*
[2]*Department of Physics, Chungbuk National University, Cheongju 28644, Republic of Korea*
[3]*Institute of Advanced Materials and Systems, Sookmyung Women's University, Seoul 04310, Republic of Korea*

(Received 21 August 2026, Received in final form 21 September 2026, Accepted 21 September 2026)

The effect of B substitution on the thermal stability and magnetic properties of $Fe_{62-x}Co_{25}Ti_7Zr_6B_x$ (x = 1–4) amorphous alloys was systematically investigated. Amorphous ribbons were fabricated by the melt-spinning technique, and their structural, thermal, and magnetic properties were characterized. XRD confirmed that all compositions retained a fully amorphous structure. As the B content increased, the first crystallization temperature increased from 508 to 566 °C, demonstrating enhanced thermal stability of the amorphous phase, whereas the coercivity decreased from 25.0 to 19.0 A/m, indicating improved soft magnetic properties. These results indicate that B substitution is an effective approach for improving the thermal stability and soft magnetic properties of Fe–Co–Ti–Zr–B amorphous alloys.

Keywords : Fe-Co amorphous ribbons, soft magnetic properties, melt-spinning, rapid solidification, magnetic domain behavior

1. Introduction

Over the past several decades, rapid industrial progress and the increasing demand for high-performance materials have accelerated the development of advanced functional materials. Among them, magnetic materials have attracted significant attention because of their broad applications in electric motors, transformers, electronic devices, information storage systems, sensors, and energy conversion technologies [1]. The continuous demand for higher efficiency and lower energy loss in these applications has driven the development of soft magnetic materials with superior magnetic performance and thermal stability.

Fe-based amorphous alloys have emerged as promising soft magnetic materials owing to their high saturation magnetization (M_S), low coercivity (H_c), high electrical resistivity, and excellent glass-forming ability (GFA). Since the successful fabrication of the Fe–P–C amorphous alloy by the melt-spinning technique in 1967 [2], extensive efforts have been devoted to developing Fe-based amorphous alloys with improved magnetic and structural properties. Among Fe-based alloys, Fe–Co alloys are particularly attractive because Co addition enhances the saturation magnetization and increases the Curie temperature, leading to improved magnetic performance, especially at elevated temperatures [3]. However, Fe–Co alloys alone exhibit relatively poor glass-forming ability, making it difficult to obtain a fully amorphous structure during rapid solidification. Therefore, the incorporation of glass-forming elements is essential to stabilize the amorphous phase while maintaining excellent magnetic properties.

Boron is one of the most effective glass-forming elements in Fe-based amorphous alloys. The addition of B increases atomic size mismatch and disrupts long-range atomic ordering, thereby suppressing crystallization and promoting amorphous phase formation [4–7]. B has been reported to enhance thermal stability by increasing the crystallization temperature and contribute to superior soft magnetic properties through the reduction of coercivity. Furthermore, Kim *et al.* reported that B addition also improves the mechanical hardness of Fe–Co–Ti–Zr–B amorphous alloys, indicating that B plays a critical role in simultaneously enhancing structural and functional properties [8]. To further improve the glass-forming ability, transition metal elements such as Ti and Zr have been

©The Korean Magnetics Society. All rights reserved.
*Corresponding author: Tel: +82-2-710-9239
E-mail: haein@sookmyung.ac.kr

widely incorporated into Fe-based amorphous alloys. The combined addition of Ti and Zr promotes the formation of metastable phases during solidification, resulting in diverse crystallization pathways that effectively suppress crystallization and stabilize the amorphous structure [9]. Consequently, the Fe–Co–Ti–Zr–B alloy system offers a favorable combination of high saturation magnetization derived from the Fe–Co matrix and enhanced glass-forming ability and thermal stability provided by B, Ti, and Zr, making it a promising candidate for advanced soft magnetic applications.

Although Fe–Co–Ti–Zr–B amorphous alloys have been extensively investigated for their soft magnetic performance and practical electromagnetic applications [10], most previous studies have focused primarily on optimizing alloy compositions or evaluating bulk magnetic properties. Although the effects of B addition on thermal stability and magnetic properties have been widely investigated, its influence on the magnetic domain behavior during the magnetization process has not yet been sufficiently clarified.

In this study, $Fe_{62-x}Co_{25}Ti_7Zr_6B_x$ (x = 1, 2, 3, and 4) amorphous alloys were investigated to systematically clarify the effect of B substitution on their thermal stability, magnetic properties, and magnetic domain behavior. Ribbon samples were fabricated using the melt-spinning technique. The magnetic properties were characterized using a vibrating sample magnetometer (VSM) and DC B–H loop measurements, while the thermal properties were analyzed by differential scanning calorimetry (DSC). Furthermore, the magnetization process and magnetic domain behavior in the amorphous ribbons were examined using the magneto-optical Kerr effect (MOKE) technique [11], providing an understanding of the influence of B substitution on the structural and magnetic characteristics of Fe–Co–Ti–Zr–B amorphous alloys.

2. Experiments and Analysis

$Fe_{62-x}Co_{25}Ti_7Zr_6B_x$ (x = 1–4) alloy ingots with a total weight of 6 g were prepared with high-purity elements Fe (99.95%), Co (99.95%), Ti (99.98%), Zr (99.95%) and B (99.5%) by arc-melting. The melting process was repeated three times to ensure chemical homogeneity of the alloys, and all melting procedures were conducted in an argon atmosphere using a Ti getter to remove residual oxygen and minimize impurities. The obtained ingots were subsequently re-melted and rapidly solidified into ribbon samples using a single-roller melt-spinning process with a rotating copper wheel. The melt-spinning parameters were set with a copper wheel speed of 38.80 m/s, a wheel-to-nozzle distance of 1 mm, a quartz nozzle diameter of 0.6 mm, and an injection pressure of 0.05 MPa.

X-ray diffraction (XRD) was used to confirm the structural properties of the ribbons using Cu-Kα radiation. The crystallization temperature (T_x) was determined using a DSC by measuring the heat flow difference between the sample and reference material under an Ar gas atmosphere. The samples were heated from room temperature to 1100 °C at a heating rate of 0.34 °C/s. The saturation magnetization (M_S) was measured along the in-plane direction using a vibrating sample magnetometer (VSM) under an applied magnetic field ranging from −10,000 to 10,000 Oe. For the VSM measurement, the ribbons were cut into approximately 5 mm lengths, and three layers of ribbons were stacked for each measurement. The coercivity (H_c) was evaluated from the B–H hysteresis loop obtained using a DC B–H loop tracer under an applied magnetic field range of −5,500 to 5,500 A/m. The acquired B-H loops consisted of data points with an average magnetic field interval of approximately 25 A/m. For the DC B–H loop tracer measurement, three to four ribbon layers were stacked to achieve a total thickness greater than 75 μm. Corresponding magnetic domain patterns and microscopic hysteresis loops were simultaneously investigated using the longitudinal magneto-optical Kerr effect (L-MOKE) microscopy. The MOKE imaging was conducted on the shiny side of the ribbons without any additional surface polishing, with the magnetic field applied along the ribbon length.

The parameters used to assess the thermodynamic tendency of the alloys were calculated from the nominal compositions. The mixing enthalpy (ΔH_{mix}), the configurational entropy of mixing (ΔS_{mix}), and the atomic size mismatch (δ) are given by

$$\Delta H_{mix} = 4\sum_{i=1}^{n}\sum_{i\neq j}^{n}\Delta H_{ij}c_i c_j \tag{1}$$

$$\Delta S_{mix} = -R\sum_{i=1}^{N} c_i \ln c_i \tag{2}$$

$$\delta = 100\sqrt{\sum_{i=1}^{N} c_i\left(1-\frac{r_i}{\bar{r}}\right)^2} \tag{3}$$

where c_i and r_i are the atomic fraction and the Goldschmidt atomic radius of the i-th element in the alloy with N elements respectively, $\bar{r} = \sum_{i=1}^{N} c_i r_i$ is the average atomic radius, R is the gas constant, and ΔH_{ij} is the binary mixing enthalpy of the i-j pair in the liquid state taken from Miedema's macroscopic atom model [12,13].

3. Results and Discussions

Fig. 1 shows the X-ray diffraction (XRD) patterns of the $Fe_{62-x}Co_{25}Ti_7Zr_6B_x$ (x = 1–4) ribbons. All compositions exhibited broad halo diffraction peaks without any detectable sharp crystalline reflections, indicating that fully amorphous ribbons were successfully fabricated over the entire compositional range. The absence of crystalline peaks demonstrates that crystallization was effectively suppressed during the melt-spinning process regardless of the B content. Since all ribbons were fabricated under identical conditions, this indicates that the cooling rate of the process was high enough to avoid crystallization in all four alloys. Boron is known to stabilize the amorphous phase rather than simply promote its formation. The increased atomic size mismatch caused by B addition hinders the development of long-range atomic ordering, and the strong chemical affinity between Fe and B enhances chemical short-range ordering and increases the energy barrier for crystallization, thereby inhibiting crystallization during rapid solidification [14].

The calculated thermodynamic parameters related to glass formation for the $Fe_{62-x}Co_{25}Ti_7Zr_6B_x$ alloys are summarized in Table 1, including ΔH_{mix}, ΔS_{mix}, and δ. These parameters are commonly used as empirical indicators of thermodynamic and topological conditions favorable for glass formation; however, they do not constitute direct experimental measures of GFA. A more negative ΔH_{mix} reflects stronger attractive interactions between unlike atoms, which promotes chemical short-range ordering and dense random packing in the liquid. Since these favorable arrangements are already present in the liquid, crystallization offers less additional energy gain. Such interactions may reduce the thermodynamic tendency toward crystallization and, together with sluggish atomic diffusion, favor the retention of the amorphous phase. In addition, the strong interactions between B and the other constituent elements increase the melt viscosity and restrict the long-range atomic diffusion required for the chemical partitioning into equilibrium intermetallic phases, so that crystallization is also suppressed kinetically. The ΔS_{mix} represents the degree of chemical disorder, where larger values generally favor the formation and stabilization of disordered amorphous structures. Meanwhile, a larger δ increases local lattice distortion, suppresses atomic diffusion, and inhibits crystal nucleation during rapid solidification. ΔH_{mix} becomes more negative and δ increases monotonically with B content, suggesting that B substitution provides thermodynamic conditions increasingly favorable for the retention of the amorphous phase. This tendency is consistent with the monotonic increase in T_{x1} described below, which provides a direct experimental measure of the thermal stability of the amorphous phase against crystallization [15].

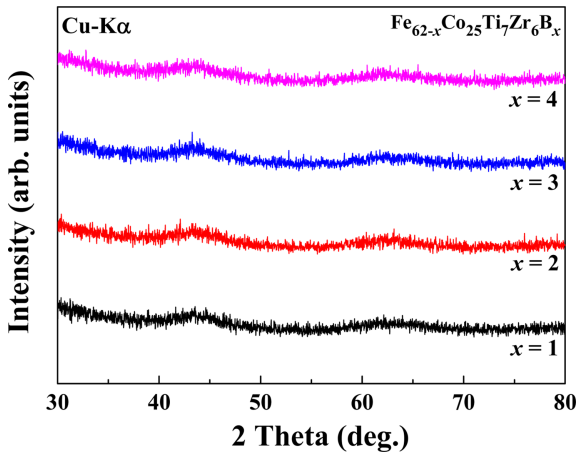


Fig. 1. (Color online) XRD (X-ray Diffraction) patterns of $Fe_{62-x}Co_{25}Ti_7Zr_6B_x$ (x = 1–4) amorphous alloys.

To evaluate the thermal stability of the amorphous ribbons, differential scanning calorimetry (DSC) measurements were performed, and the results are presented in Fig. 2. All compositions exhibited distinct exothermic peaks corresponding to the first crystallization temperature (T_{x1}). As listed in Table 1, T_{x1} increased systematically from 508 °C for x = 1 to 566 °C for x = 4 with increasing B content. The increase in T_{x1} indicates that greater

Table 1. Magnetic, thermal properties and thermodynamic parameters related to glass formation of $Fe_{62-x}Co_{25}Ti_7Zr_6B_x$ (x = 1–4) alloys.

x	Composition	Magnetic Properties		Thermal Property	Thermodynamic parameters related to glass formation		
		M_S (emu/g)	H_c (A/m)	T_x (°C)	ΔH (kJ/mol)	ΔS (J/mol·K)	δ (%)
1	$Fe_{61}Co_{25}Ti_7Zr_6B_1$	142	25.0	508	-12.8	8.34	8.61
2	$Fe_{60}Co_{25}Ti_7Zr_6B_2$	136	22.0	545	-13.9	8.38	9.12
3	$Fe_{59}Co_{25}Ti_7Zr_6B_3$	136	23.2	554	-14.9	8.42	9.60
4	$Fe_{58}Co_{25}Ti_7Zr_6B_4$	131	19.0	566	-16.0	8.46	10.1

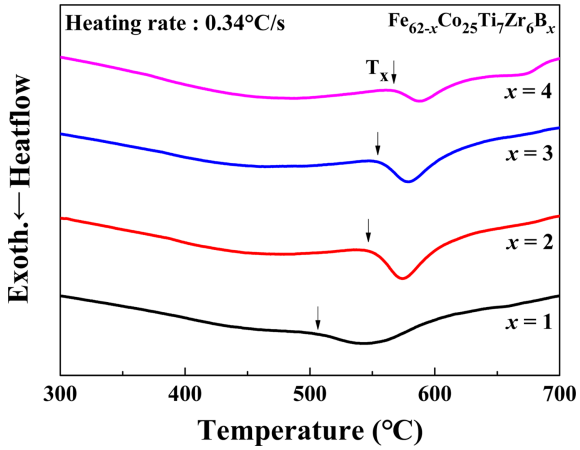


Fig. 2. (Color online) Crystallization curves of $Fe_{62-x}Co_{25}Ti_7Zr_6B_x$ (x = 1–4) amorphous ribbons measured by DSC.

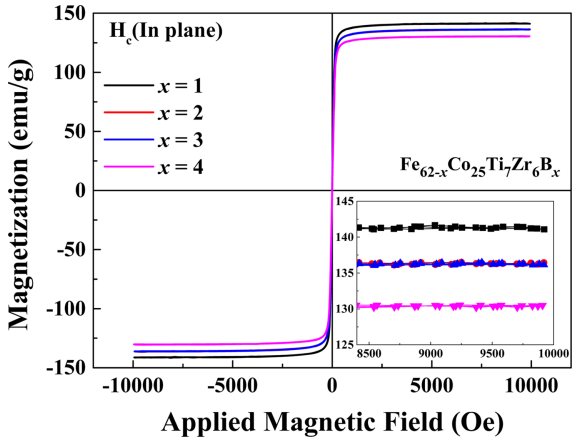


Fig. 3. (Color online) Magnetic hysteresis curves measured by VSM for $Fe_{62-x}Co_{25}Ti_7Zr_6B_x$ (x = 1–4) amorphous ribbons.

thermal energy is required to initiate crystallization, suggesting that the amorphous structure becomes increasingly resistant to crystallization with increasing B content. This behavior is consistent with the thermodynamic parameters related to glass formation. The strong chemical interaction between Fe and B atoms restricts atomic diffusion, while the increased atomic size mismatch suppresses structural rearrangement during heating, thereby delaying the formation and growth of crystalline nuclei. Consequently, boron significantly enhances the thermal stability of the amorphous phase against subsequent thermal exposure. The improved thermal stability is advantageous for soft magnetic materials because it enables the amorphous structure and its associated magnetic properties to be retained over a wider operating temperature range.

The magnetic properties of the $Fe_{62-x}Co_{25}Ti_7Zr_6B_x$ ribbons were characterized using a vibrating sample magnetometer (VSM) and a DC B–H loop tracer. Fig. 3 shows the magnetization curves measured by VSM. The saturation magnetization decreased gradually from 142 emu/g at x = 1 to 131 emu/g at x = 4 as the B content increased. This decrease is mainly attributed to the substitution of ferromagnetic Fe atoms by non-magnetic B atoms. Since Fe is the primary contributor to the magnetic moment of this alloy system, reducing the Fe concentration inevitably lowers the overall saturation magnetization. Therefore, although boron improves the structural stability of the amorphous phase, increasing its content accompanies a trade-off in magnetic performance by slightly reducing M_S.

The coercivity (H_c) values measured using the DC B–H loop tracer are also summarized in Table 1. The coercivity exhibited an overall decreasing tendency with increasing B content, with a slight increase at x = 3 followed by a

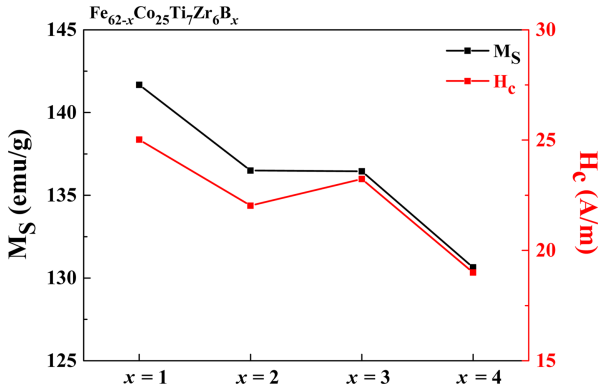


Fig. 4. (Color online) Dependence of saturation magnetization (M_S) and coercivity (H_c) on B content of $Fe_{62-x}Co_{25}Ti_7Zr_6B_x$ (x = 1–4) alloys.

further decrease at x = 4, as shown in Fig. 4, exhibiting an inverse relationship with M_S. This slight deviation in H_c indicates that the effect of B addition on the coercivity is not strictly monotonic. Unlike the monotonic reduction in M_S, the overall decrease in H_c indicates that boron improves the soft magnetic properties of the alloy system. In an amorphous ferromagnet, the coercivity is governed by the residual effective anisotropy <K> through

$$H_c \approx p_c \cdot \frac{<K>}{M_S} \tag{4}$$

where p_c is a dimensionless factor of order unity. Since magnetocrystalline anisotropy is absent, <K> originates mainly from the magnetoelastic contribution $\frac{3}{2}\lambda_s\sigma$, where λ_s is the saturation magnetostriction and σ is the internal stress [16]. Since M_S decreases with B content and appears in the denominator, the reduction in M_S alone would raise H_c; the fact that H_c decreases therefore indicates that <K> falls more rapidly than M_S. A change

in the magnetoelastic contribution, associated with composition-dependent magnetostriction and quenched-in residual stress, is a plausible explanation for the decrease in coercivity. However, because neither magnetostriction nor residual stress was measured directly, the dominant contribution cannot be identified from the present results. Direct measurements of magnetostriction and residual stress would therefore be required to clarify the dominant mechanism. Therefore, although increasing the B content slightly sacrifices saturation magnetization, it improves the magnetic softness of the alloy system.

Although the VSM and DC B–H loop measurements quantitatively reveal the changes in M_S and H_c, they do not directly explain the magnetization reversal process responsible for the observed improvement in coercivity. Since coercivity is closely related to the nucleation and propagation of magnetic domains, direct observation of magnetic domain behavior is necessary to clarify the underlying magnetization mechanism. Therefore, magneto-optical Kerr effect (MOKE) microscopy observations were performed to investigate the magnetic domain structures and local magnetic hysteresis loops and to clarify the magnetization reversal mechanism responsible for the observed magnetic properties.

As shown in Fig. 5, all compositions exhibited relatively low coercivity. The coercivity of $Fe_{61}Co_{25}Ti_7Zr_6B_1$ was approximately 3.9 Oe (310 A/m), whereas the other compositions exhibited values near 3.0 Oe (240 A/m), decreasing slightly with increasing B content as shown in the enlarged loops in Fig. 5(b). These coercivity results differ from those obtained using the DC B–H loop tracer, which may be attributed to differences in the measurement area of the samples and measurement method between the two techniques. MOKE probes only the surface region within a limited field of view, whereas the B–H tracer averages the flux over the entire volume of the stacked ribbons, so the two methods sample different parts of the switching field distribution. The Kerr images revealed complex and irregular domain configurations, without a regular stripe pattern in every composition. Such configu-

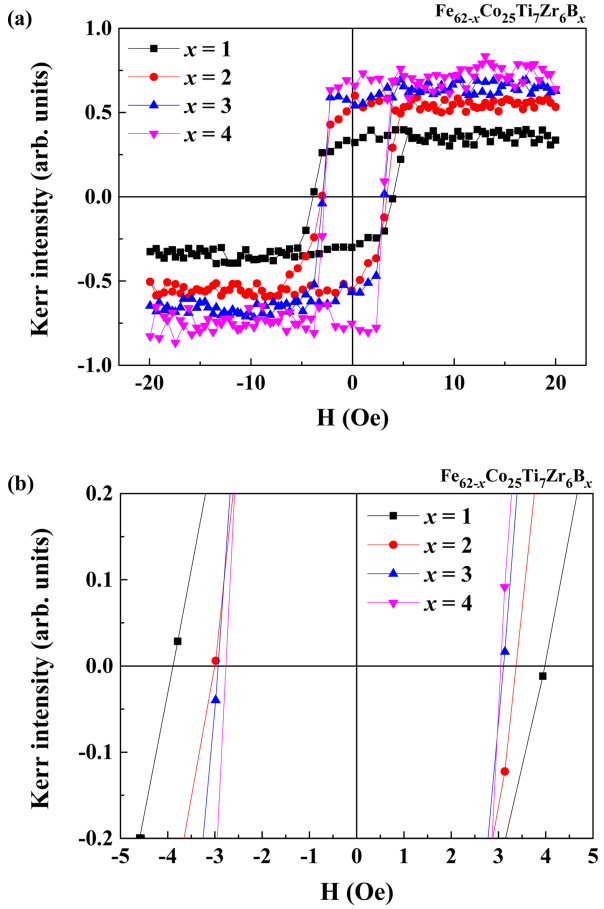


Fig. 5. (Color online) (a) Kerr hysteresis loops of all compositions, and (b) enlarged Kerr hysteresis loops near the coercive field.

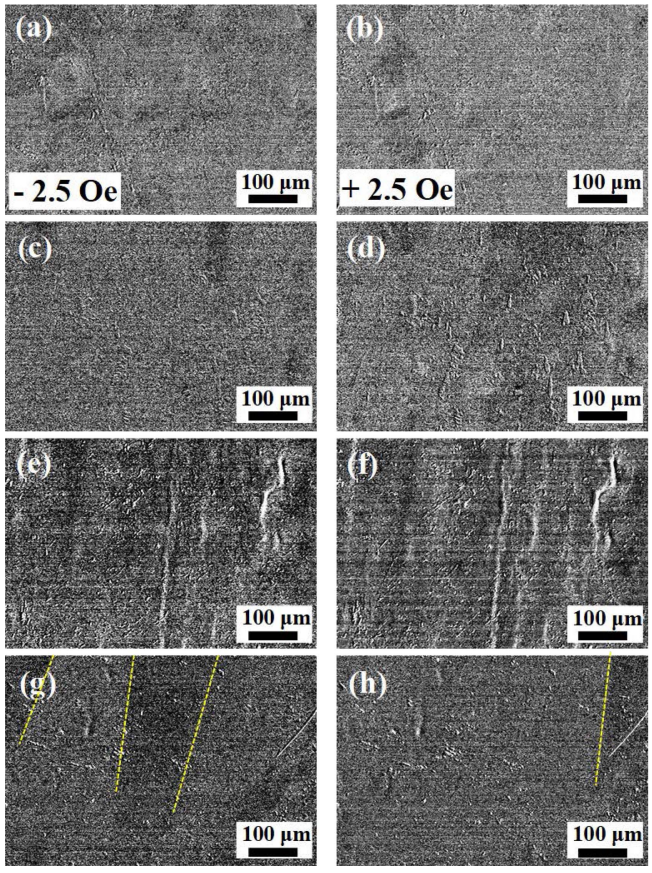


Fig. 6. (Color online) Kerr magnetic domain images of $Fe_{62-x}Co_{25}Ti_7Zr_6B_x$ (x = 1–4) under (a, c, e, g) negative and (b, d, f, h) positive external magnetic fields: (a, b) x = 1, (c, d) x = 2, (e, f) x = 3, (g, h) x = 4.

rations are typical of melt-spun amorphous ribbons. Because the ribbon is quenched rapidly, residual stress is frozen in non-uniformly across the sample. Since the Fe-rich amorphous matrix has a non-zero magnetostriction, this stress sets the local easy axis, which therefore points in different directions from place to place [11]. Fig. 6 shows the Kerr domain images of all four compositions under negative and positive external magnetic fields. The contrast and configuration of the domain regions differ between the negative and positive field states in every composition, and the domain boundaries are slightly better defined in $Fe_{58}Co_{25}Ti_7Zr_6B_4$ than in the other samples. These irregular domain configurations appear in both field states, suggesting that magnetization reversal is not dominated by simple, uniform domain-wall motion but instead reflects a spatially distributed magnetization-reversal process involving multiple domain regions. The slight increase at x = 3 seen in the bulk H_c is not observed in the Kerr loops. This difference further indicates that the local surface-sensitive MOKE response does not necessarily follow the volume-averaged magnetic response of the stacked ribbons. The domain configurations, however, remain irregular and similar in character in all compositions, with no systematic change as the B content increases. This indicates that the reduction in H_c is not accompanied by an appreciable change in the domain structure. The improvement in soft magnetic properties is therefore better explained by the reduction in <K> discussed above than by a decrease in the number of domain-wall pinning sites, which would be expected to alter the domain configurations.

4. Conclusions

The experimental results obtained in this study clearly demonstrate the influence of B content on the thermal stability and magnetic properties of $Fe_{62-x}Co_{25}Ti_7Zr_6B_x$ (x = 1–4) amorphous alloys. The main findings are summarized as follows:

- All $Fe_{62-x}Co_{25}Ti_7Zr_6B_x$ ribbons exhibited a fully amorphous structure throughout the investigated composition range. Increasing the B content enhanced the thermal stability of the amorphous phase, as evidenced by the increase in the first crystallization temperature from 508 to 566 °C.
- Although the saturation magnetization gradually decreased with increasing B content because of the reduced Fe content, the coercivity also decreased from 25.0 to 19.0 A/m, indicating an improvement in the soft magnetic properties. Since M_S decreases at the same time, the reduction in coercivity requires the effective anisotropy <K> to decrease more rapidly than M_S, suggesting that a reduction in the effective anisotropy, possibly involving the magnetoelastic contribution, plays an important role.
- The present results demonstrate that B substitution effectively enhances the thermal stability while simultaneously improving the soft magnetic properties of Fe–Co–Ti–Zr–B amorphous alloys at the cost of a modest reduction in saturation magnetization. Therefore, controlling the B content provides an effective means of tailoring the thermal stability and magnetic performance of this alloy system.
- MOKE observations showed that the domain configurations remained irregular and similar in all compositions, indicating that the decrease in coercivity does not originate from a change in the domain structure.

Acknowledgement

This work was supported by the National Research Foundation of Korea (NRF) grant funded by the Korea government (MSIT) (RS-2025-00564040). PD & DHK acknowledge Institute of Information & Communications Technology Planning & Evaluation (IITP) - Information Technology Research Center (ITRC) research grant funded by the Korea government (Ministry of Science and ICT) number IITP-2025-RS-2024–0043728.

References

[1] Z. Liu, Metals **13**, 1318 (2023).
[2] P. Duwez and S. C. H. Lin, J. Appl. Phys. **38**, 4096 (1967).
[3] J. Wang, Z. Wang, Y. Jia, R. Shi, and Z. Wen, J. Magn. Magn. Mater. **328**, 62 (2013).
[4] S. Kim, B.-K. Han, J.-Y. Suh, S.-D. Kim, D.-H. Kim, Y. K. Kim, and H. Choi-Yim, Intermetallics **90**, 164 (2017).
[5] H. Koshiba, A. Inoue, and A. Makino, J. Appl. Phys. **85**, 5136 (1999).
[6] K. Suzuki, A. Makino, A.-P. Tsai, A. Inoue, and T. Masumoto, Materials Science and Engineering: A **179**, 501 (1994).
[7] K. Suzuki, N. Kataoka, A. Inoue, A. Makino, and T. Masumoto, Materials Transactions, JIM **31**, 743 (1990).
[8] S. Kim, B. K. Han, D. T. Quach, D.-H. Kim, Y. K. Kim, and H. Choi-Yim, Current Applied Physics **16**, 515 (2016).
[9] J. Si, C. Du, T. Wang, Y. Wu, R. Wang, and X. Hui, J. Alloys Compd. **741**, 542 (2018).
[10] H. W. Chang, Y. C. Huang, C. W. Chang, C. C. Hsieh, and W. C. Chang, J. Alloys Compd. **472**, 166 (2009).
[11] Z. Hussain, S. H. Babu, and V. R. Reddy, J. Non. Cryst. Solids **571**, 121073 (2021).

[12] A. Takeuchi and A. Inoue, Materials Transactions **46**, 2817 (2005).
[13] A. Takeuchi, K. Amiya, T. Wada, K. Yubuta, W. Zhang, and A. Makino, Entropy **15**, 3810 (2013).
[14] N. Chen, L. Martin, D. V. Luzguine-Luzgin, and A. Inoue, Materials **3**, 5320 (2010).
[15] R. Busch, J. Schroers, and W. H. Wang, MRS Bulletin **32**, 620 (2007).
[16] T. Hysen, S. Al-Harthi, I. A. Al-Omari, P. Geethaa, R. Lisha, R. V. Ramanujan, D. Sakthikumar, and M. R. Anantharaman, J. Magn. Magn. Mater. **341**, 165 (2013).